Applied Surface Science 505 (2020) 144612

Contents lists available at ScienceDirect

Applied Surface Science

journal homepage: www.elsevier.com/locate/apsusc

Full Length Article

Surface coating of MOF layers on the nanocrystals of other MOFs using nanoparticle mediated nucleation for the efficient removal of formaldehyde

Raekyung Kim[1], UnJin Ryu[1], Seohyeon Jee, Kyung Min Choi*

Department of Chemical and Biological Engineering, Sookmyung Women's University, 100 Cheongpa-ro 47 gil, Yongsan-gu, Seoul 04310, Republic of Korea

ARTICLE INFO

Keywords:
MOF coating
Nanocrystalline metal-organic frameworks
Nanoparticles
Water sorption
Formaldehyde removal

ABSTRACT

The coating of metal-organic frameworks (MOFs) has been desired to control the surrounding environment of the substrate and the pathway for the guest molecules approaching. Especially, the MOF layer coating on the other MOF nanoparticles has been challenging because of lattice mismatch and undesired homogeneous nucleation. In this report, we coated MOF layers on other nanocrystalline MOFs (nMOFs) using metal nanoparticle mediated nucleation method, and showed how this coating can be used for unique sorption behavior of H_2O and efficient removal of trace formaldehyde existing in ppm level in air. Specifically, the layers of MOF-801 and UiO-66 were grown from the Pt nanoparticles attached on the particles of nUiO-66 and nMOF-801 to result final products of nMOF-801 ⊂ UiO-66 and nUiO-66 ⊂ MOF-801, respectively. We found that these samples of nUiO-66 ⊂ MOF-801 and nMOF-801 ⊂ UiO-66 present unusual H_2O uptake behaviors originated from the sequence of condensation between inner and outer MOFs. These samples also captured 7 times higher amount of formaldehyde than an activated carbon and had high affinity to release less amount of formaldehyde even when its concentration outside is low.

1. Introduction

The coating of metal-organic frameworks (MOFs) on various substrates has provided advantages of changing the surrounding environment of the substrate as well as of controlling the behavior of guest molecules approaching to the substrate [1–12]. This is because MOFs have highly porous structures providing open accessibility to outside and high degree of flexibility with which their physical and chemical properties can be varied by manipulating their constituents of metal oxides and organic ligands [13–17]. In this reason, the coating MOFs has been explored to various materials of metals, metal oxides, semiconductors, and polymers usually using surface modification and direct-growth of MOF [18–21]. However, the challenge remains for the MOF coating on the surface of a different MOF especially when their lattice parameters are different [21–26]. When the parameters are not matched, organic mediators had been necessarily used to cover outside of particles increasing the attractive interaction with the MOF layer coated on [23,24], which remained at the interface of the coated structure and inevitably effected on the guest molecule transfer. We believe that the direct conjunction of two different MOF structures at the interface would provide opportunities for making unique properties with the guest molecules.

In this study, we report a surface coating method of MOF layers by nucleating them from metal nanoparticles spatially distributed on the nanocrystalline MOFs (nMOFs) (Fig. 1). Specifically, the nanocrystalline MOF-801 [27] and UiO-66 [28] particles (hereafter referred to as nMOF-801 and nUiO-66, respectively) were prepared and Pt nanoparticles are subsequently attached on them to give intermediate products of Pt-**on**-nMOF-801 and Pt-**on**-nUiO-66, respectively. The surface coating of UiO-66 and MOF-801 was successfully mediated from the nanoparticle of Pt-**on**-nMOF-801 and Pt-**on**-nUiO-66 to result final products of nMOF-801 ⊂ UiO-66 and nUiO-66 ⊂ MOF-801 (Fig. 1). The coating structure, morphology, crystallinity, porosity and the coating ratio of nMOF-801 ⊂ UiO-66 and nUiO-66 ⊂ MOF-801 were characterized using transmission electron microscopy (TEM), scanning electron microscopy (SEM), powder X-ray diffraction (PXRD), N_2 sorption and ^1H nuclear magnetic resonance spectrometer (NMR) analysis. The *ex-situ* TEM observation of nMOF-801 ⊂ UiO-66 revealed the details for the nucleation and growth process of coated UiO-66 on the surface of nMOF-801 particle. The samples of nMOF-801 ⊂ UiO-66 and nUiO-66 ⊂ MOF-801 were tested for the sorption of H_2O and CO_2, which led us to find out the unusual behavior of these samples in relation with the gas condensation. This finding was also connected to the efficient and non-emittable removal of trace formaldehyde in air. The

* Corresponding author.
E-mail address: kmchoi@sookmyung.ac.kr (K.M. Choi).
[1] Raekyung Kim and UnJin Ryu contributed to the work equally.

https://doi.org/10.1016/j.apsusc.2019.144612
Received 26 September 2019; Received in revised form 31 October 2019; Accepted 4 November 2019
Available online 09 November 2019
0169-4332/

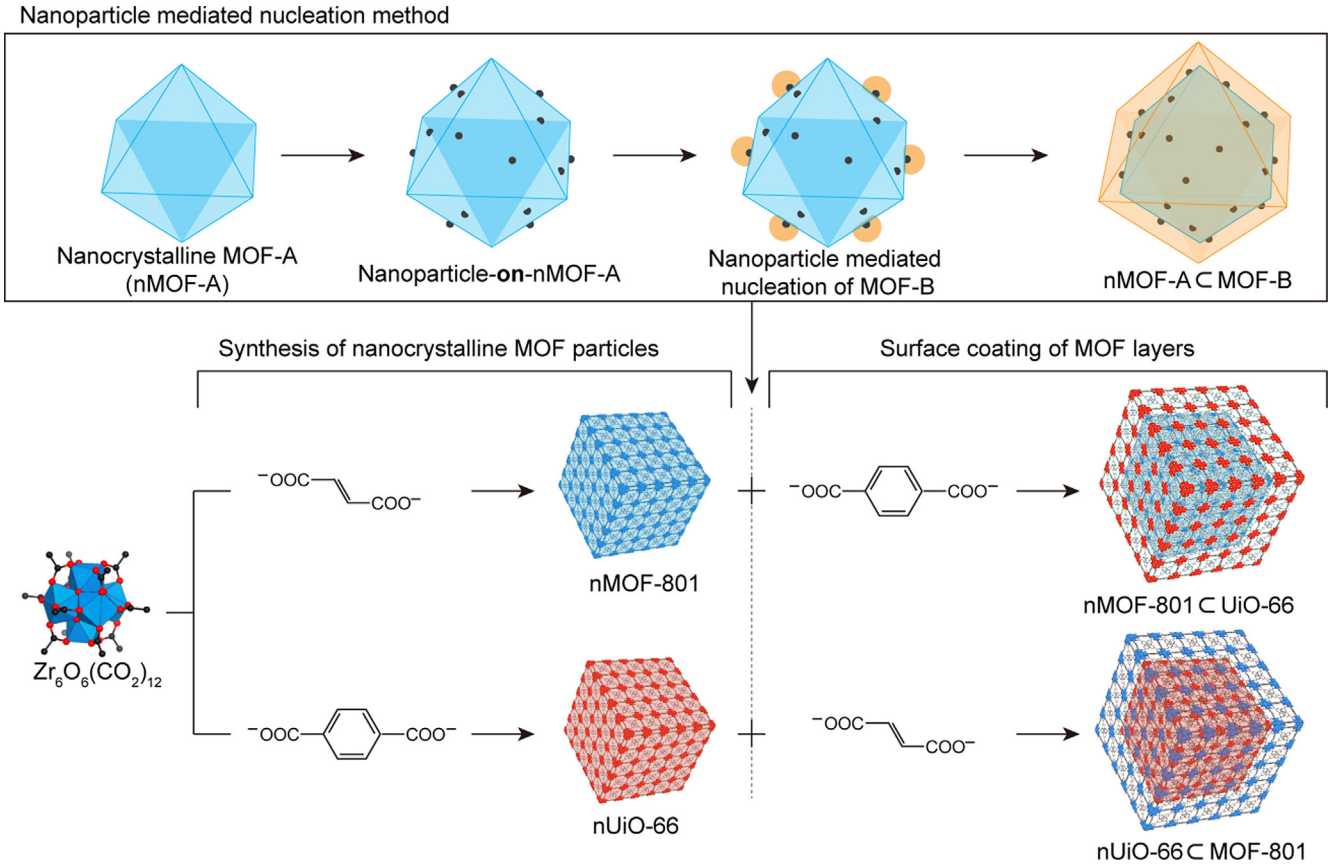

Fig. 1. Schematic diagram of nanoparticle mediated nucleation method and synthetic procedure of nMOF-801 ⊂ UiO-66 and nUiO-66 ⊂ MOF-801.

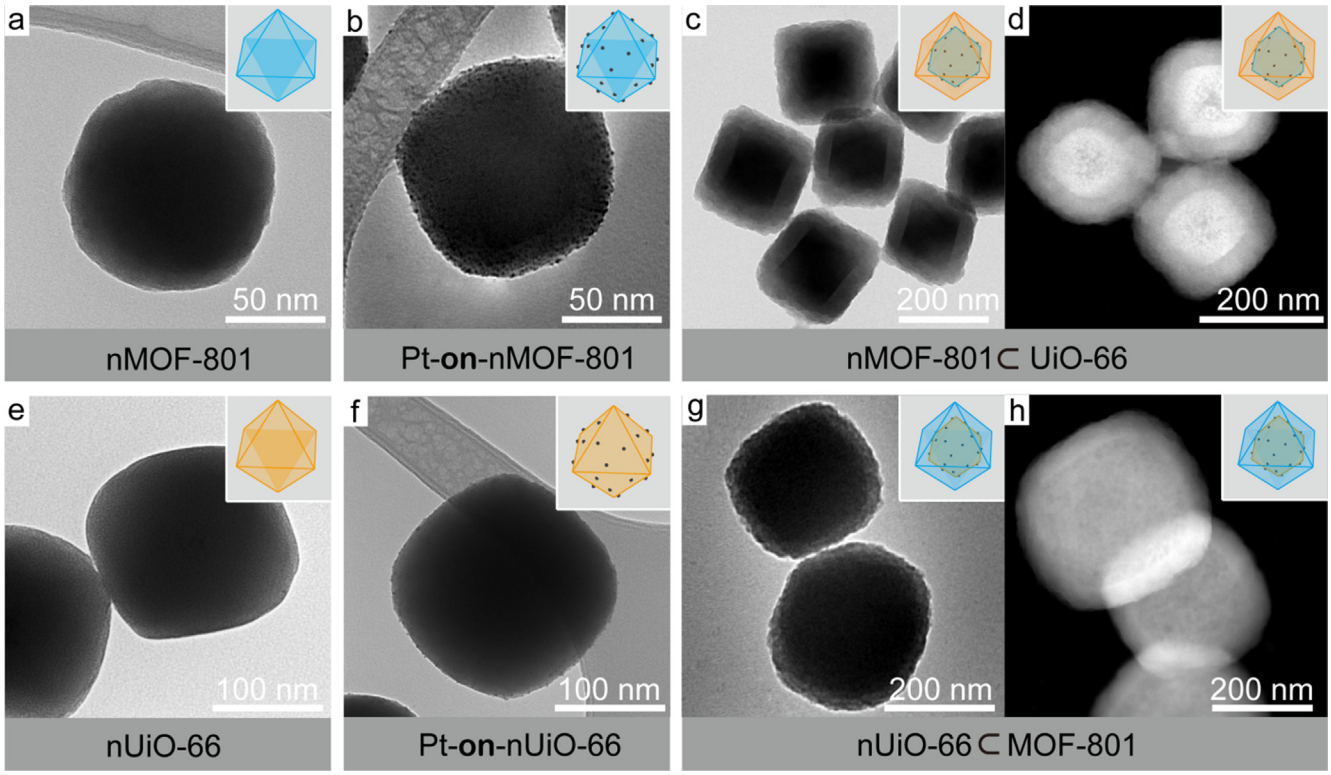

Fig. 2. TEM and STEM images of (a) nMOF-801, (b) Pt-on-nMOF-801, (c for TEM and d for STEM images) nMOF-801 ⊂ UiO-66, (e) nUiO-66, (f) Pt-on-nUiO-66, and (g for TEM and h for STEM images) nUiO-66 ⊂ MOF-801.

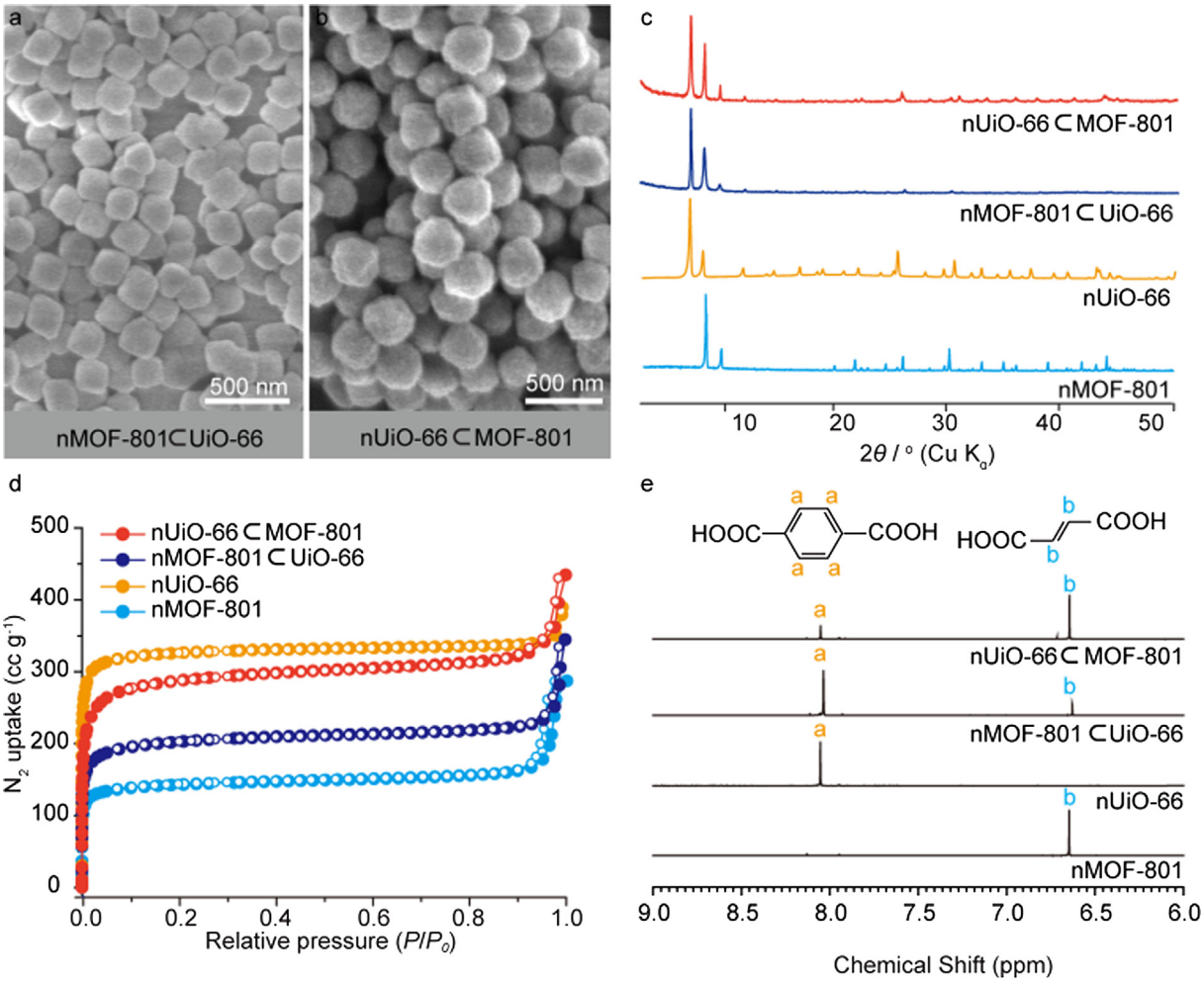

Fig. 3. Characterization of nMOF-801 ⊂ UiO-66 and nUiO-66 ⊂ MOF-801 samples. (a and b) SEM images nMOF-801 ⊂ UiO-66 and nUiO-66 ⊂ MOF-801 samples, (c) PXRD patterns, (d) N_2 sorption isotherms at 77 K (adsorption and desorption points represented by closed circles and open circles, respectively, and P/P_0 is relative pressure), and (e) ^{1}H NMR spectrum of digested samples of nMOF-801 ⊂ UiO-66 and nUiO-66 ⊂ MOF-801 in comparison with those of nUiO-66 and nMOF-801.

samples of nMOF-801 ⊂ UiO-66 and nUiO-66 ⊂ MOF-801 showed 7 times higher amount of uptake than activated carbon and high affinity to release less amount of the formaldehyde even in lower outside concentration.

2. Materials and methods

2.1. Materials

All reagents were used without further purification. Specifically, zirconium chloride (IV), fumaric acid, terephthalic acid (H_2BDC), acetic acid, *N,N'*-dimethylformamide (DMF), methanol (MeOH), poly(vinylpyrrolidone) (PVP), ethylene glycol, chloroplatinic acid hexahydrate ($H_2PtCl_6{\cdot}6H_2O$) were purchased from Sigma-Aldrich.

2.2. Materials preparation

Synthesis of Pt nanoparticle: H_2PtCl_6 (40 mg) was added into 20 ml of ethylene glycol and poly(vinyl pyrrolidone) (PVP, MW = 55,000) (222 mg) mixture with stirring in a three-neck round bottomed flask. When the solution became homogeneous, the flask was heated in silicon bath at 180 °C for 15 min and cooling down to room temperature. The product was washed with acetone to remove the extra PVP and separated solvent with centrifuge. The collected black PVP-capped Pt NPs were re-dispersed in DMF to give colloidal solution (1 mg/mL).

Synthesis of nanocrystalline MOFs (nMOFs): For nMOF-801, $ZrCl_4$ (66.8 mg) and fumaric acid (36 mg) were dissolved in the mixture of DMF/acetic acid (10 ml/1.38 ml) in 20 ml vial and placed 120 °C oven for 6 h. For nUiO-66, $ZrCl_4$ (66.8 mg) and terephthalic acid (49.8 mg) were dissolved in the mixture of DMF/acetic acid (10 ml/1.38 ml) in 20 ml vial and placed 120 °C oven for 3 h. After cooling to room temperature, the powder products were collected by centrifuging (4000 rpm, 10 min) and washed with DMF once and with MeOH 3 times. After washing, it was dried under 120 °C vacuum and obtained white powder product.

Preparation of Pt-on-nMOF-A: For Pt-on-nMOF-801, the 5 ml of MOF-801 stock solution (13.7 mg/ml) and 0.375 ml of Pt NPs (1 mg/ml) solution was added into 20 ml of DMF. For Pt-on-nUiO-66, the 5 ml of UiO-66 solution (13.7 mg/ml) and 0.75 ml of Pt NPs (1 mg/ml) solution was added into 40 ml of DMF. The mixture sonicated for 5 h. After sonication, the vial cooled down at room temperature and washed with DMF three times using centrifuge. After washing, gray powder was dissolved in 20 ml of DMF as stock solution.

Synthesis of nMOF-A ⊂ MOF-B: For nMOF-801 ⊂ UiO-66, $ZrCl_4$ (83.5 mg) and terephthalic acid (62.5 mg) was dissolved in DMF/Acetic acid (50 ml/1.75 ml), followed by the 8 ml of Pt-on-nMOF-801 stock solution was added in the solution. For nUiO-66 ⊂ MOF-801, $ZrCl_4$ (167 mg) and fumaric acid (90 mg) was dissolved in DMF/Acetic acid (50 ml/3.5 ml) followed by the 1 ml of Pt-on-nUiO-66 stock solution

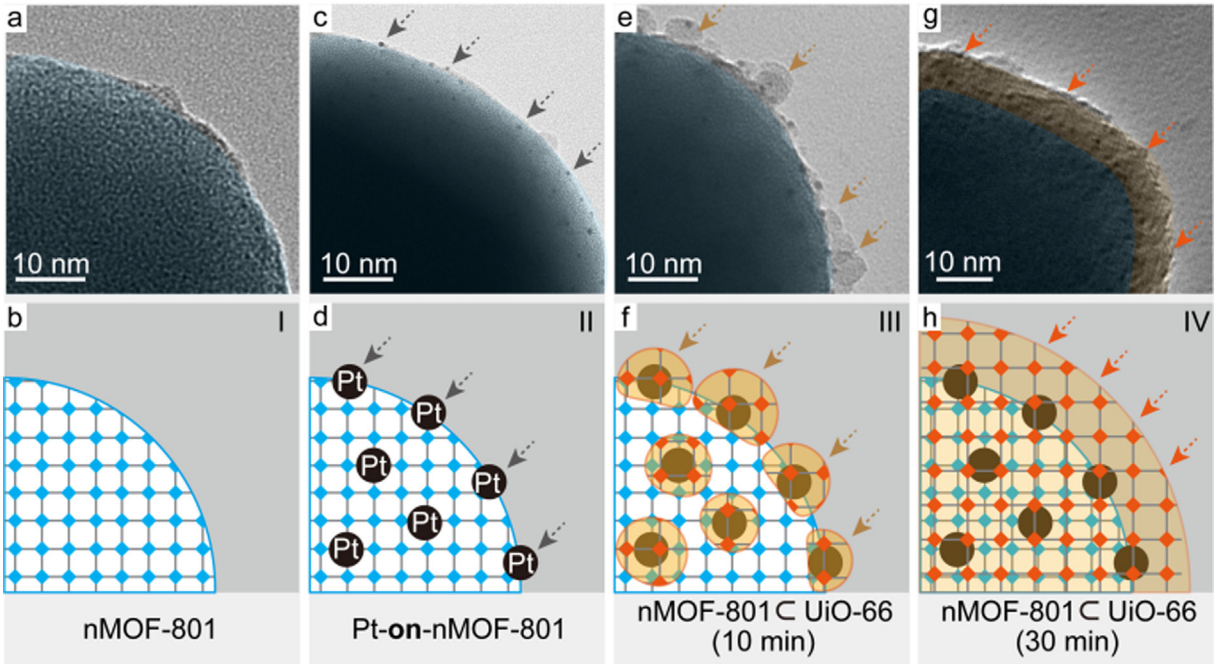

Fig. 4. The *ex-situ* TEM observation of surface coating process in nMOF-801 ⊂ UiO-66. The TEM images and schemes of (a and b) nMOF-801, (c and d) Pt-on-nMOF-801, (e and f) nMOF-801 ⊂ UiO-66 (10 min), and (g and h) nMOF-801 ⊂ UiO-66 (30 min).

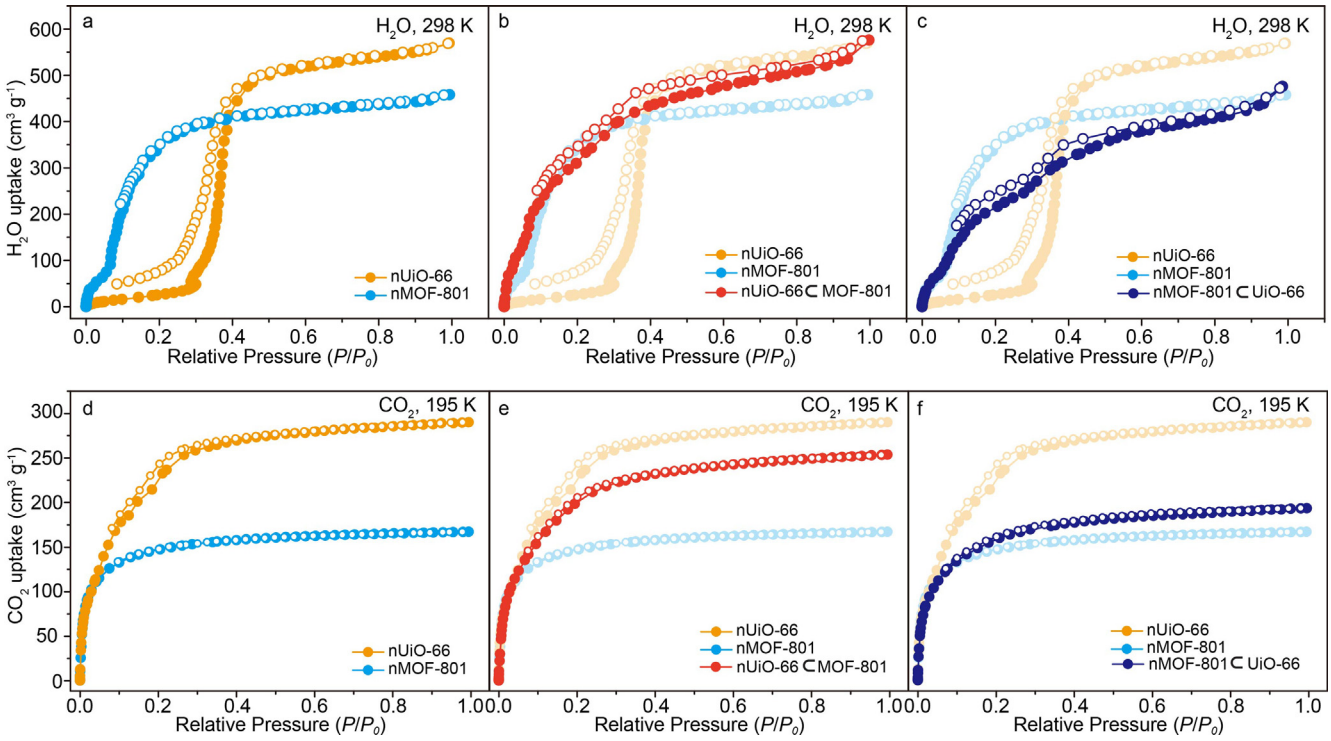

Fig. 5. H_2O sorption isotherm of (a) nMOF-801 and nUiO-66 (b) nUiO-66 ⊂ MOF-801 and (c) nMOF-801 ⊂ UiO-66 measured at 298 K. CO_2 sorption isotherm of (d) nMOF-801 and nUiO-66 (e) nUiO-66 ⊂ MOF-801 and (f) nMOF-801 ⊂ UiO-66 measured at 195 K.

was added in the solution. Each reaction was placed in 100 ml round bottomed flask at 120 °C with stirring for 1 h and 1.5 h for nMOF-801 ⊂ UiO-66 and nUiO-66 ⊂ MOF-801, respectively. After reaction, the products were washed with DMF twice and MeOH 3 times. Finally, the resulting powder was obtained after removing the solvent under 120 °C vacuum for 12 h.

2.3. Characterization

Powder X-ray diffraction patterns (PXRD) were detected using a Bruker D8 Advance diffractometer (Cu Kα radiation λ = 1.54056 Å). The samples were held in a non-reflective holder stage with Göbel-mirror monochromated mode and scanned by 5°/min scan speed in continuous mode (40 KV, 40 mA). The SEM observations (JSM-7600F JEOL) were carried out in GB_LOW mode, with a WD of 8.0 mm and

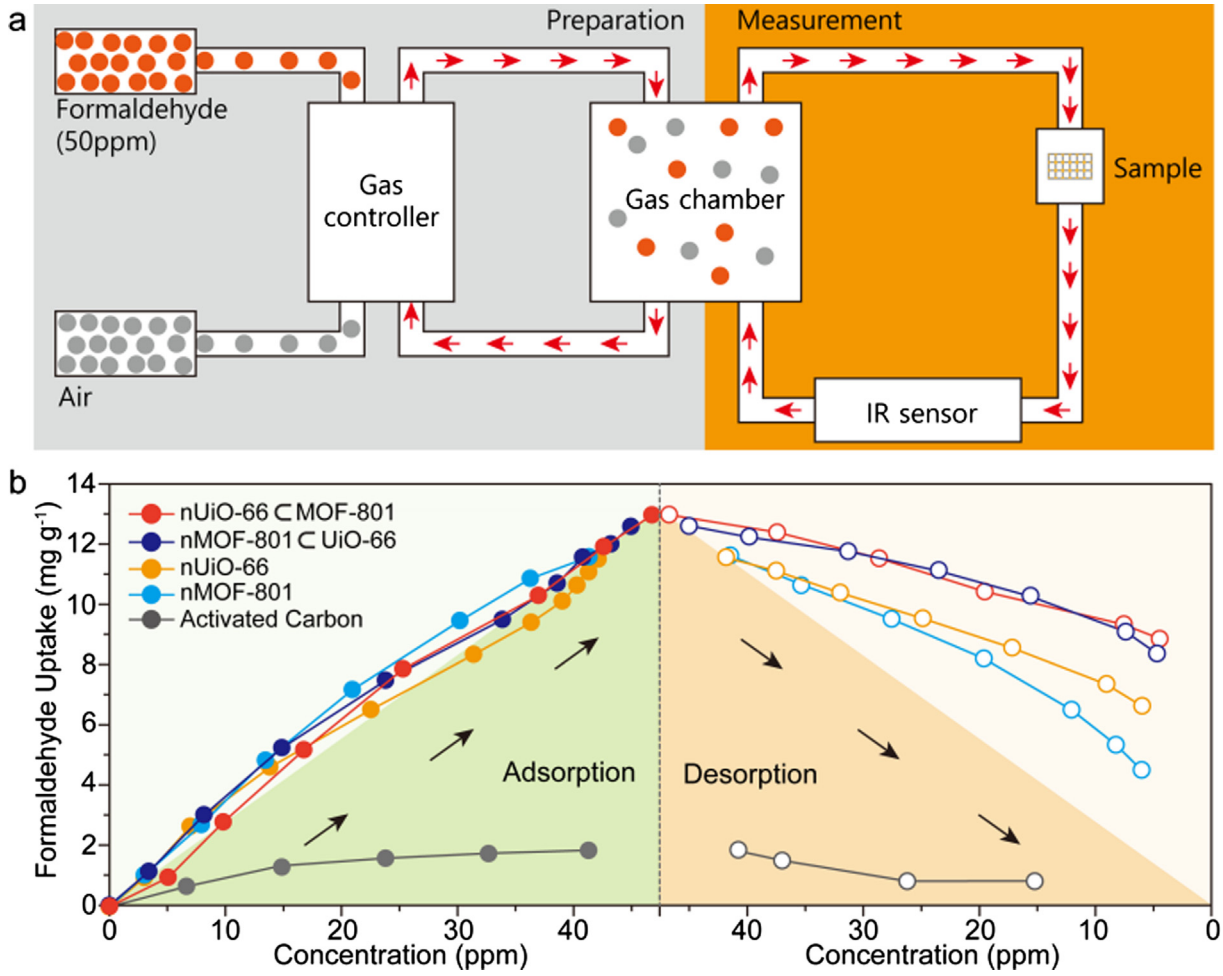

Fig. 6. Adsorption and desorption of formaldehyde for the samples of nMOF-801, nUiO-66, nUiO-66 ⊂ MOF-801, nMOF-801 ⊂ UiO-66 and activated carbon.

scanned by 3 kV. For the TEM observation, samples are first dispersed in acetone using sonicator and drop to cupper square grid. Observation was carried out in the TEM (JEOL JEM-2100F.) with 200 kV. ^{1}H NMR analysis of digested nMOFs were detected with a Bruker Avance III HD 500 NMR spectrometer. To prepare the measuring samples, 3 mg of dried MOF powder was digested and dissolved in the mixture of DMSO-d_6 (570 μL) and hydrofluoric acid (30 μL) with sonication. Gas adsorption analysis was performed using a BELSOPR-max (MicrotracBEL Corp.) gas adsorption analyzer. Samples were prepared and measured after evacuating at 120 °C for 24 h. Formaldehyde sorption method was measured by photoacoustic sensor with a customized instrument. Total 20 steps processed 1 step per 90 min adsorption and 90 min desorption time. Before measurement, 30 mg powder samples was activated 120 °C vacuum oven for 24 h.

3. Results and discussion

The samples of nMOF-801 and nUiO-66 particles were prepared using a mixture of DMF solution containing $ZrCl_4$, acetic acid and organic linkers. The organic linker of nMOF-801 is fumaric acid and that of nUiO-66 is terephthalic acid, which two linkers have different length between carboxylic acid in both ends. The mixtures were kept at 120 °C for 3 and 6 h to synthesize nanoparticles of nMOF-801 and nUiO-66. The resulting solution became pale white and the powder-type products was sedimentated at the bottom of a reactor. The white nanoparticles were obtained after washing with DMF and MeOH, followed by drying under vacuum. The crystallinity of nMOF-801 and nUiO-66 was examined by powder X-ray diffraction (PXRD) (Figure S1), which showed sharp diffraction peaks matching those of their simulated patterns obtained from experimental X-ray single-crystal diffraction data [13,29,30]. The permanent porosity of nMOF-801 and nUiO-66 was also confirmed by measuring the nitrogen gas sorption isotherm. It showed shapes similar to those observed for these MOFs and gave BET surface areas of 550 and 1300 m^2/g for nMOF-801 and nUiO-66, respectively (Figure S2). The TEM images of nMOF-801 and nUiO-66 showed crystal sizes of 100 nm and 200 nm with octahedron shape, respectively (Fig. 2a and e). This is also corresponding to their SEM images with high crystal size and shape uniformity (Figure S3).

Monodisperse Pt nanoparticles (NPs) are synthesized with H_2PtCl_6 and poly(vinylpyrrolidone) (PVP) stabilizer in ethylene glycol. Pt NPs were characterized by TEM images, which shows Pt NPs are well monodispersed with 3.5 nm in diameter. Pt nanoparticles (NPs) were diluted to 1 wt% DMF solution and are attached on the outside of nMOF-801 and nUiO-66 particles using an ultra-sonication to give Pt-**on**-nMOF-801 and Pt-**on**-nUiO-66 as shown in Fig. 2b and f. After Pt NPs treatments, the color of nanocrystalline MOFs was changed from white to gray due to the deposition of black Pt NPs. Pt NPs could not interpenetrate into the nMOF-801 particles as their size (3.5 nm) is much bigger than the pore size of MOF-801 (0.74 nm) and UiO-66 (0.84 nm) [13]. These Pt NPs were used as nucleation points for the next-step coating of another MOF.

Thin layers of UiO-66 and MOF-801 were coated on the outside of Pt-**on**-nMOF-801 and Pt-**on**-nUiO-66 to give nMOF-801 ⊂ UiO-66 and nUiO-66 ⊂ MOF-801, respectively (Fig. 2). The particles of Pt-**on**-nUiO-66 and Pt-**on**-nMOF-801 were well-dispersed in DMF using an ultra-sonication, and then mixed with $ZrCl_4$ and corresponding organic

linkers (terephthalic acid for UiO-66 coating and fumaric acid for MOF-801 coating). These mixtures were placed in 120 °C oil bath and stirred during the coating reactions. After cooling to room temperature, the MOFs were washed with DMF and MeOH by centrifuging with 4000 rpm. It was activated under vacuum for 1 day and the white powder were obtained. The coating structure of resulting particles were revealed by TEM and scanning transmission electron microscopy (STEM) observation as shown in Fig. 2c and d for nMOF-801 ⊂ UiO-66, and Fig. 2g and h for nUiO-66 ⊂ MOF-801. TEM images present the interface of two different MOF layers and STEM images clearly show that outer layer is homogeneously coated on the surface of core particle in the samples of nMOF-801 ⊂ UiO-66 (Fig. 2d) and nUiO-66 ⊂ MOF-801 (Fig. 2h). The thickness of coated layer is *ca.* 50 nm for both samples, which was able to be controlled by mean of reaction time for coated MOF layer (Figure S4 and S5). The final sizes of nMOF-801 ⊂ UiO-66 and nUiO-66 ⊂ MOF-801 were about 200 nm and 300 nm, respectively. It is noteworthy that the coating of surface MOF layer wasn't successful without deposition of Pt NP in the identical synthetic protocol including sonication and nMOF dispersion processes, due to the lattice mismatch between MOF-801 and UiO-66 structures.

The size and morphology uniformity of nMOF-801 ⊂ UiO-66 and nUiO-66 ⊂ MOF-801 samples was investigated with SEM observation (Fig. 3a and b). Every particles from same batch of reactor has homogeneous particle size. This is corresponding to the observation confirmed in the TEM above (Fig. 2c and g). Sharp PXRD diffraction patterns present that the samples of nMOF-801 ⊂ UiO-66 and nUiO-66 ⊂ MOF-801 have high crystallinity and diffraction peaks corresponding to both of nMOF-801 and nUiO-66 (Fig. 3c). The nMOF-801 ⊂ UiO-66 and nUiO-66 ⊂ MOF-801 samples have intense peaks at $2\theta = 7.4^{\circ}$, 8.5° and 9.9°, which were corresponding to the peaks for MOF-801 ($2\theta = 8.5^{\circ}$ and 9.9°) and UiO-66 ($2\theta = 7.4^{\circ}$ and 8.5°). The permanent porosity of the nMOF-801 ⊂ UiO-66 and nUiO-66 ⊂ MOF-801 are confirmed with N_2 adsorption measured at 77 K after activating pores under vacuum at 120 °C for overnight [31,32]. The nMOF-801 ⊂ UiO-66 and nUiO-66 ⊂ MOF-801 maintained high porosity even after MOF layer coating and showed characteristic type I adsorption isotherm behavior similar to their constituents. It was considered that N_2 molecules were not blocked at the interface of two MOF layers and diffused well into inner nMOFs. The nMOF-801 ⊂ UiO-66 has slightly higher BET surface area (770 m^2/g) than nMOF-801 (550 m^2/g) while nUiO-66 ⊂ MOF-801 (1120 m^2/g) shows a slightly lower value than nUiO-66 (1300 m^2/g) [33]. The samples were subjected to digested-NMR measurement which is a technique analyzing the organic parts after breaking down the MOF structure by dissolving the metal oxide parts. The MOFs samples were digested with HF in DMSO-d_6 by sonication, and ^{1}H NMR spectra are collected on a 500 MHz Bruker NMR spectrometer. ^{1}H NMR analysis for the digested samples of nMOF-801 ⊂ UiO-66 and nUiO-66 ⊂ MOF-801 demonstrated that they were consisted with two kinds of linkers, fumaric acid and terephthalic acid. The nMOF-801 ⊂ UiO-66 and nUiO-66 ⊂ MOF-801 have peaks at (a) 8.1 ppm and (b) 6.8 ppm corresponding to terephthalic acid for UiO-66 and fumaric acid for MOF-801, respectively [34]. The integration of these peaks shows that the molar ratio of MOF-801 layer coated on nUiO-66 is 66.6 mol% in nUiO-66 ⊂ MOF-801 sample while that of UiO-66 layer on nMOF-801 is 86.5 mol% in nMOF-801 ⊂ UiO-66 sample. These ratios are corresponding to the core-to-shell volume ratios of 70% and 87.5% for each sample.

An *ex-situ* TEM observation of nMOF-801 ⊂ UiO-66 samples gave an insight for the formation of coated UiO-66 layer from the Pt NP outside of nMOF-801. We prepared 4 kinds of samples as nMOF-801, Pt-**on**-nMOF-801, nMOF-801 ⊂ UiO-66 reacted 10 min, and nMOF-801 ⊂ UiO-66 reacted 30 min of coating process. The surface of prepared samples were sequentially observed using a high-resolution TEM as shown in Fig. 4. The surface of nMOF-801 was smooth and homogenous (Fig. 4a and b) while that of Pt-**on**-nMOF-801 showed Pt NPs attached on it (Fig. 4c and d). The Pt NPs was confirmed to exist outside of nMOF-801 not inside. The Pt-**on**-nMOF-801 particles are mixed with terephthalic acid and $ZrCl_4$ in DMF and then the coating process of UiO-66 was started by placing them in oven. After 10 min of surface coating process, nMOF-801 ⊂ UiO-66 (10 min) particles were taken out and subjected to TEM observation. The TEM image of nMOF-801 ⊂ UiO-66 (10 min) (Fig. 4e) clearly shows that nuclei of UiO-66 started to form from the Pt NP attached on the nMOF-801 particle (Fig. 4f). This indicates that our nanoparticle mediated nucleation approach successfully works for the MOF coating even on the surface of another MOF having lattice parameter mismatched. The coated layer of UiO-66 on nMOF-801 was observed after 30 min reaction and its thickness was about 8 nm (Fig. 4g and h). Longer reaction time for the coating process resulted thicker layer of UiO-66 (Figure S4). The reaction longer than 70 min in coating process also induced homogeneous nucleation UiO-66 to result nUiO-66 particles existing together with nMOF-801 ⊂ UiO-66 particles.

As the nMOF-801 and nUiO-66 particles are encapsulated by the layer of UiO-66 and MOF-801, respectively, guest molecules have to go through the cover layers in samples of nMOF-801 ⊂ UiO-66 and nUiO-66 ⊂ MOF-801. We hypothesized that our samples would show unique sorption behavior once the condensation of guest molecules is started from the outer coating layer and then propagate to inner part, while the other way should show step-by-step gas condensation behavior. Furthermore, the guest molecule having similar condensation behavior in both inner and outer part wouldn't show any uniqueness but marginal total uptake. We have choose two gases of H_2O and CO_2 to test our samples of nMOF-801, nUiO-66, nUiO-66 ⊂ MOF-801 and nMOF-801 ⊂ UiO-66 and their sorption isotherms are shown in Fig. 5. The nMOF-801 and nUiO-66 showed completely different H_2O condensation pressure ($P/P_0 = 0.01$ and 0.1 for nMOF-801 and $P/P_0 = 0.3$ for nUiO-66) (Fig. 5a), while similar CO_2 condensation pressure regime under $P/P_0 = 0.2$ (Fig. 5d). The uUiO-66 showed higher total uptake than nMOF-801 for both H_2O and CO_2 (Fig. 5a and d). In case of H_2O uptake, nUiO-66 ⊂ MOF-801 showed gradual condensation behavior from $P/P_0 = 0.0$ to $P/P_0 = 0.4$ and then its total amount of uptake approach to that of nUiO-66 from $P/P_0 = 0.4$ (Fig. 5b). This is contrast to the case of nMOF-801 ⊂ UiO-66 showing three-step condensation behavior originated from each of nMOF-801 at $P/P_0 = 0.01$ and 0.1 and nUiO-66 at $P/P_0 = 0.3$, sequentially (Fig. 5c). We speculate that this is because the sample of nUiO-66 ⊂ MOF-801 has the H_2O condensation started from the outer layer of MOF-801 then propagated into inner part of nUiO-66 while nMOF-801 ⊂ UiO-66 has sequential condensation from the inner nMOF-801 to the outer UiO-66. In case of CO_2 uptake, the uptake behavior of nMOF-801 ⊂ UiO-66 and nUiO-66 ⊂ MOF-801 was similar to that of nMOF-801 and nUiO-66 while their total amount of uptake was intermediate (Fig. 5d–f). These results imply that the coating of MOF layer induces unusual uptake behavior in conjunction with the gas condensation.

The unique sorption behavior of nUiO-66 ⊂ MOF-801 and nMOF-801 ⊂ UiO-66 combined with the condensation of guest molecules led us to use this compounds for the removal of formaldehyde which is self-condensable gas forming oligomers spontaneously. The removal of formaldehyde has been challenging because it is toxic trace gas existing in ppm level in air and, once captured, should not get out from its absorbent. We believed that the uniqueness of our compound combined with the condensation of formaldehyde give a chance to remove the formaldehyde in air. Moreover, it was expected that the homogeneous micropores of MOFs effectively capture the formaldehyde comparing to conventional porous carbon samples. The adsorption and desorption of the samples are measured in a closed-loop system having a large gas-mixing chamber connected to a sample and a gas detector (1512i photoacoustic gas monitor, LumaSense Technology) at room temperature (Fig. 6a). The concentration of formaldehyde in air was controlled by mixing formaldehyde gas and air using gas controller. When the mixed gas in the gas chamber was equilibrated at target concentration, it flowed through the sample while the supply from outside was blocked

to make a closed-loop circulation system (Fig. 6a). The difference between initial and final concentration of formaldehyde was calculated to get the amount of sorption per a gram of sample. For the adsorption of formaldehyde, all samples of nMOF-801, nUiO-66, nUiO-66 ⊂ MOF-801 and nMOF-801 ⊂ UiO-66 showed similar behavior (Fig. 6b). The amount of uptake for these samples also captured 7 times higher was proportional to the surrounding concentration and 7 times higher than that for commercial activated carbon (Fig. 6b). It was considered that the microporosity of these MOF samples efficiently capture formaldehyde inside comparing to the carbon sample. On the contrary, the desorption behavior for nUiO-66 ⊂ MOF-801 and nMOF-801 ⊂ UiO-66 was different with that for MOF-801 and nUiO-66. When surrounding air has lower concentration in desorption process, the MOF samples release less amount of the formaldehyde than they adsorbed (Fig. 6b). Especially, nUiO-66 ⊂ MOF-801 and nMOF-801 ⊂ UiO-66 release much less amount than the samples of nMOF-801 and nUiO-66. We speculate that this is because the condensation of formaldehyde at the outer MOF layer interrupt the gas transfer from inside in desorption process. By utilizing this unique sorption behavior, the nUiO-66 ⊂ MOF-801 and nMOF-801 ⊂ UiO-66 can efficiently remove the formaldehyde without re-emission in each cycle and be used again after activation for recycles (Table S1). We expect that the coating of MOF layer on other MOF particles would provide further unique behavior for the removal and conversion of harmful gases in the air.

4. Conclusion

MOF layers were coated on other nanocrystalline MOF particles using metal nanoparticle mediated nucleation method. Specifically, nanocrystalline particles of nMOF-801 and nUiO-66 were synthesized and combined with Pt nanoparticle to give a nucleation point for next-step MOF layer coating. We confirmed that UiO-66 layer and MOF-801 layer were successfully nucleated from the Pt nanoparticles and then covered entire nMOF-801 and nUiO-66 particles to give nMOF-801 ⊂ UiO-66 and nUiO-66 ⊂ MOF-801, respectively. The *ex-situ* TEM observation proved that the growth of outer MOF layer was mediated from the metal nanoparticles. We also found that these samples of nUiO-66 ⊂ MOF-801 and nMOF-801 ⊂ UiO-66 present a unique uptake behavior in conjunction with the condensation of guest molecules. Especially, the nUiO-66 ⊂ MOF-801 sample showed the unique H_2O sorption behavior totally different to the samples of nMOF-801 and nUiO-66 while the nMOF-801 ⊂ UiO-66 sample showed step-by-step sorption behavior corresponding to nMOF-801 and nUiO-66. This was originated from the sequence of condensation between inner and outer parts: outer-to-inner for the nUiO-66 ⊂ MOF-801 and inner-to-outer for the nMOF-801 ⊂ UiO-66. These unique sorption behavior was connected to the non-emittable formaldehyde removal. The samples of nUiO-66 ⊂ MOF-801 and nMOF-801 ⊂ UiO-66 captured large amount of formaldehyde while releasing less amount to the outside than the samples of nMOF-801 and nUiO-66. We believe that the synthetic strategy in this report would open the possibility constructing different core-shell structures using MOFs and other organic/inorganic nanoparticles based on a new level of heterogeneity within order to make unexpected properties. Moreover, the compounds reported here can be applied to the removal and catalytic conversion of environmental harmful gases.

Acknowledgments

This work was supported by the Basic Science Research Program (NRF-2019R1A2C4069764).

Declaration of Competing Interest

The authors declare that they have no known competing financial interests or personal relationships that could have appeared to influence the work reported in this paper. The authors declare the following financial interests/personal relationships which may be considered as potential competing interests.

Appendix A. Supplementary material

Supplementary data to this article can be found online at https://doi.org/10.1016/j.apsusc.2019.144612.

References

[1] F. Jeremias, St. K. Henninger, C. Janiak, High performance metal–organic-framework coatings obtained via thermal gradient synthesis, Chem. Commun. 48 (2012) 9708–9710, https://doi.org/10.1039/C2CC34782B.
[2] R.A. Fischer, A. Bétard, Metal-organic framework thin films: from fundamentals to applications, Chem. Rev. 112 (2012) 1055–1083, https://doi.org/10.1021/cr200167v.
[3] D. Farrusseng, Metal-Organic Frameworks: Applications from Catalysis to Gas Storage, Willy-VCH, Weinheim, 2011.
[4] J. Gascon, F. Kapteijn, Metal-organic framework membranes-high potential, bright future? Angew. Chem. Int. Ed. 49 (2010) 1530–1532, https://doi.org/10.1002/anie.200906491.
[5] C.M. Lew, R. Cai, Y. Yan, Zeolite thin films: from computer chips to space stations, Acc. Chem. Res. 43 (2010) 210–219, https://doi.org/10.1021/ar900146w.
[6] M.A. Snyde, M. Tsapatsis, Hierarchical nanomanufacturing: from shaped zeolite nanoparticles to high-performance separation membranes, Angew. Chem. Int. Ed. 46 (2007) 7560–7573, https://doi.org/10.1002/anie.200604910.
[7] O. Shekhah, J. Liu, R.A. Fischer, Ch. Wöell, MOF thin films: existing and future applications, Chem. Soc. Rev. 40 (2011) 1081–1106, https://doi.org/10.1039/c0cs00147c.
[8] J.-L. Zhuang, A. Terfort, C. Wöll, Formation of oriented and patterned films of metal–organic frameworks by liquid phase epitaxy: a review, Coord. Chem. Rev. 307 (2016) 106–129, https://doi.org/10.1016/j.ccr.2015.09.013.
[9] Y.-R. Lee, J. Kim, W.-S. Ahn, Synthesis of metal-organic frameworks: a mini review, Korean J. Chem. Eng. 30 (2013) 1667–1680, https://doi.org/10.1007/s11814-013-0140-6.
[10] N. Jiang, Z. Deng, S. Liu, C. Tang, G. Wang, Synthesis of metal organic framework (MOF-5) with high selectivity for CO_2/N_2 separation in flue gas by maximum water concentration approach, Korean J. Chem. Eng. 33 (2016) 2747–2755, https://doi.org/10.1007/s11814-016-0092-8.
[11] S. Bae, N. Zaini, K.S.N. Kamarudin, K.S. Yoo, J. Kim, M.R. Othman, Rapid solvothermal synthesis of microporous UiO-66 particles for carbon dioxide capture, Korean J. Chem. Eng. 35 (2018) 764–769, https://doi.org/10.1007/s11814-017-0334-4.
[12] H. Jeong, R. Roshan, R. Babu, H.J. Kim, D.W. Park, Zirconium-based isoreticular metal-organic frameworks for CO_2 fixation via cyclic carbonate synthesis, Korean J. Chem. Eng. 35 (2018) 438–444, https://doi.org/10.1007/s11814-017-0294-8.
[13] H. Furukawa, F. Gándara, Y. Zhang, J. Jiang, W.L. Queen, M.R. Hudson, O.M. Yaghi, Water adsorption in porous metal-organic frameworks and related materials, J. Am. Chem. Soc. 136 (2014) 4369–4381, https://doi.org/10.1021/ja500330a.
[14] S. Abednatanzi, P.G. Derakhshandeh, H. Depauw, F. Coudert, H. Vrielinck, P. Van Der Voort, K. Leus, Mixed-metal metal–organic frameworks, Chem. Soc. Rev. 48 (2019) 2535–2565, https://doi.org/10.1039/C8CS00337H.
[15] L.J. Wang, H.X. Deng, H. Furukawa, F. Gandara, K.E. Cordova, D. Peri, O.M. Yaghi, Synthesis and characterization of Metal-organic framework-74 containing 2, 4, 6, 8, and 10 different Metals, Inorg. Chem. 53 (2014) 5881–5883, https://doi.org/10.1021/ic500434a.
[16] S. Yuan, L. Feng, K. Wang, J. pang et al. Stable metal–organic frameworks: design, synthesis, and applications, Adv. Mat. 30 (2018) 1704303. https://doi.org/10.1002/adma.201704303.
[17] Z. Yin, Y. Zhou, M. Zeng, M. Kurmoo, The concept of mixed organic ligands in metal–organic frameworks: design, tuning and functions, Dalton Trans. 44 (2015) 5258–5275, https://doi.org/10.1039/C4DT04030A.
[18] G. Huang, D.M. Yin, L.M. Wang, A general strategy for coating metal–organic frameworks on diverse components and architectures, J. Mater. Chem. A 4 (2016) 15106–15116, https://doi.org/10.1039/C6TA05389K.
[19] P. Hu, J. Zhuang, L.Y. Chou, H.K. Lee, X.Y. Ling, Y.C. Chuang, C.K. Tsung, Surfactant-directed atomic to mesoscale alignment: metal nanocrystals encased individually in single-crystalline porous nanostructures, J. Am. Chem. Soc. 136 (2014) 10561–10564, https://doi.org/10.1021/ja5048522.
[20] J. Zhuang, L.Y. Chou, B.T. Sneed, Y. Cao, P. Hu, L. Feng, C.K. Tsung, Surfactant-mediated conformal overgrowth of core-shell metal–organic framework materials with mismatched topologies, Small 11 (2015) 5551–5555, https://doi.org/10.1002/smll.201501710.
[21] R. Kim, S. Jee, U. Ryu, H.S. Lee, S.Y. Kim, K.M. Choi, Surface-enhanced infrared detection of benzene in air using a porous metal-organic-frameworks film, Korean J. Chem. Eng. 36 (2019) 975–980, https://doi.org/10.1007/s11814-018-0231-0.
[22] H. Furukawa, U. Müller, O.M. Yaghi, "Heterogeneity within order" in metal-organic frameworks, Angew. Chem. Int. Ed. 54 (2015) 3417–3430, https://doi.org/10.1002/anie.201410252.
[23] K. Ikigaki, K. Okada, Y. Tokudome, T. Toyao, P. Falcaro, C.J. Doonan,

M. Takahashi, MOF-on-MOF: oriented growth of multiple layered thin films of metal-organic frameworks, Angew. Chem. Int. Ed. 58 (2019) 6886–6890, https://doi.org/10.1002/anie.201901707.
[24] Z. Wang, J. Liu, B. Lukose, Z. Gu, P.G. Weidler, H. Gliemann, T. Heine, C. Wöll, Nanoporous designer solids with huge lattice constant gradients: multi-heteroepitaxy of metal-organic frameworks, Nano Lett. 14 (2014) 1526–1529, https://doi.org/10.1021/nl404767k.
[25] O. Shekhah, K. Hirai, H. Wang, H. Uehara, S.M. Kondo, S. Diring, D. Zacher, R.A. Fischer, O. Sakata, S. Kitagawa, S. Furukawa, C. Wöll, MOF-on-MOF hetero-epitaxy: perfectly oriented $[Zn_2(ndc)_2(dabco)]_n$ grown on $[Cu_2(ndc)_2(dabco)]_n$ thin films, Dalton Trans. 40 (2011) 4954–4958, https://doi.org/10.1039/C0DT01818J.
[26] M. Zhao, K. Yuan, Y. Wang, G.D. Li, J. Guo, L. Gu, W.P. Hu, H. Zhao, Z. Tang, Metal-organic frameworks as selectivity regulators for hydrogenation reactions, Nature 539 (2016) 76–80, https://doi.org/10.1038/nature19763.
[27] G. Wißmann, A. Schaate, S. Lilienthal, I. Bremer, A.M. Schneider, P. Behrens, Modulated synthesis of Zr-fumarate MOF, Micropor. Mesopor. Mat. 152 (2012) 64–70, https://doi.org/10.1016/j.micromeso.2011.12.010.
[28] J.H. Cavka, S. Jakobsen, U. Olsbye, N. Guillou, C. Lamberti, S. Bordiga, K.P. Lillerud, A new zirconium inorganic building brick forming metal organic frameworks with exceptional stability, J. Am. Chem. Soc. 130 (2008) 13850–13851, https://doi.org/10.1021/ja8057953.
[29] S. Øien, D. Wragg, H. Reinsch, S. Svelle, S. Bordiga, C. Lamberti, K.P. Lillerud, Detailed structure analysis of atomic positions and defects in zirconium metal-organic frameworks, Cryst. Growth Des. 14 (2014) 5370–5372, https://doi.org/10.1021/cg501386j.
[30] Q. Li, Q. Liu, J. Zhao, Y. Hua, J. Sun, J. Duan, W. Jin, High efficient water/ethanol separation by a mixed matrix membrane incorporating MOF filler with high water adsorption capacity, J. Membrane. Sci. 544 (2017) 68–78, https://doi.org/10.1016/j.memsci.2017.09.021.
[31] F. Fathieh, M.J. Kalmutzki, E.A. Kapustin, P.J. Waller, J. Yang, O.M. Yaghi, Practical water production from desert air, Sci. Adv. 4 eaat3198 (2018), https://doi.org/10.1126/sciadv.aat3198.
[32] F. Zhang, S. Zheng, Q. Xiao, Y. Zhong, W. Zhu, A. Lin, M.S. El-Shall, Synergetic catalysis of palladium nanoparticles encaged within amine-functionalized UiO-66 in the hydrodeoxygenation of vanillin in water, Green chem. 9 (2016) 2900–2908, https://doi.org/10.1039/C5GC02615F.
[33] X. Min, X. Wu, P. Shao, Z. Ren, L. Ding, X. Luo, Ultra-high capacity of lanthanum-doped UiO-66 for phosphate capture: unusual doping of lanthanum by the reduction of coordination number, Chem. Eng. J. 358 (2019) 321–330, https://doi.org/10.1016/j.cej.2018.10.043.
[34] J. Aguilera-Sigalat, A. Fox-Charles, D. Bradshaw, Direct photo-hydroxylation of the Zr-based framework UiO-66, Chem. Comm. 50 (2014) 15453–15456, https://doi.org/10.1039/C4CC07882A.